Time-Resolved Infrared Spectroscopic Study of Reactive Acyl Intermediates Relevant to Cobalt-Catalyzed Carbonylations[1]

Steven M. Massick,[†] Julienne G. Rabor,[†] Stefan Elbers,[†] Jon Marhenke,[†] Stefan Bernhard,[‡] Jon R. Schoonover,[‡] and Peter C. Ford*,[†]

Department of Chemistry, University of California, Santa Barbara, California 93106, and Bioscience/ Biotechnology Group (CST-4), Chemical Science and Technology Division, Los Alamos National Laboratory, Los Alamos, New Mexico 87545

Time-resolved infrared spectroscopic studies have been used to characterize the reactive intermediate $CH_3C(O)Co(CO)_2$-PPh_3 ($\mathbf{I_{Co}}$), which is relevant to the mechanism of the catalysis of alkene hydroformylation by the phosphine-modified cobalt carbonyls. Step-scan FTIR and (variable) single-frequency time-resolved infrared detection on the microsecond time scale were used to record the spectrum of $\mathbf{I_{Co}}$ and to demonstrate that the principal photoproduct of the subsequent reaction of this species at $P_{CO} = 1$ atm is the methyl cobalt complex CH_3Co-$(CO)_3PPh_3$ ($\mathbf{M_{Co}}$). At higher P_{CO} the trapping of $\mathbf{I_{Co}}$ with CO to re-form $CH_3C(O)Co(CO)_3PPh_3$ ($\mathbf{A_{Co}}$) (rate $= k_{CO}[CO][\mathbf{I_{Co}}]$) was shown to become competitive with the rate of acetyl-to-cobalt methyl migration to give $\mathbf{M_{Co}}$ (rate $= k_M[\mathbf{I_{Co}}]$). Activation parameters for the competing pathways in benzene were determined to be $\Delta H^{\ddagger}_{CO} = 5.7 \pm 0.4$ kJ mol^{-1}, $\Delta S^{\ddagger}_{CO} = -91 \pm 12$ J mol^{-1} K^{-1} and $\Delta H^{\ddagger}_{M} = 40 \pm 2$ kJ mol^{-1}, $\Delta S^{\ddagger}_{M} = -19 \pm 5$ J mol^{-1} K^{-1}. The effects of varying the solvent on the competitive reactions of $\mathbf{I_{Co}}$ were also explored, and the mechanistic implications of these results are discussed.

Introduction

Carbonylation catalysis has been a major component of the chemical industry since the discovery of homogeneous cobalt carbonyl catalysts for alkene hydroformylation in 1938 by Otto Roelen at Ruhrchemie AG.[2,3] The original hydroformylation catalysts were based on simple cobalt carbonyl precursors; however, a phosphine-modified cobalt catalyst having a more favorable linear-to-branched selectivity has been developed.[2,3] Although rhodium catalysis is now predominant for propene hydroformylation, cobalt-catalyzed processes continue to be important for the hydroformylation of higher olefins owing to the greater thermal stability of the cobalt catalysts at temperatures necessary for separating higher boiling products.[3] In addition there is continuing interest in new applications of cobalt carbonyls as catalysts for syn-gas reactions.[4−6]

Pioneering studies by Heck and Breslow[7] of alkene hydroformylation of alkenes led to the proposed catalytic cycle illustrated by Scheme 1, and this model has served as the starting point for quantitative reaction mechanism studies of various aspects of unsubstituted and substituted cobalt carbonyl

Scheme 1. Proposed Mechanism for Homogeneous Cobalt-Catalyzed Hydroformylation
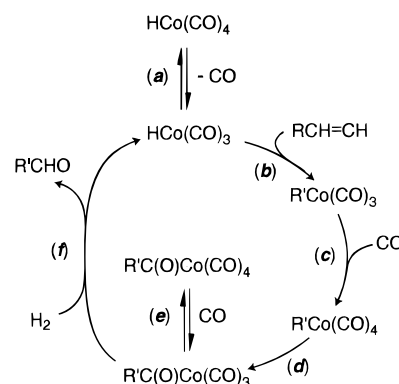
catalysts.[8−17] A key step in that scheme is the migratory insertion of a CO into a Co−R bond (step 1d). This is the fundamental carbon−carbon bond formation pathway in this and other

[†] University of California, Santa Barbara.

[‡] Los Alamos National Laboratory.

(1) Reported in part at the 217th ACS National Meeting, Anaheim CA, March 1999, INORG 168, and at the 213th ACS National Meeting, San Francisco CA, April 1997, INORG 141.

(2) Parshall, G. W.; Ittel, S. D. *Homogeneous Catalysis*; John Wiley & Sons: New York, 1992.

(3) Cornils, B.; Herrmann, W. A. *Applied homogeneous catalysis with organometallic compounds: a comprehensive handbook in two volumes*; VCH: Weinheim, New York, 1996.

(4) Knifton, J. F.; Lin, J. J. *J. Mol. Catal.* **1993**, *81*, 27−36.

(5) Piotti, M. E.; Alper, H. *J. Am. Chem. Soc.* **1996**, *118*, 111−116.

(6) Rathke, J. W.; Klinger, R. J.; Krause, T. R. *Organometallics* **1991**, *10*, 1350−1355.

(7) Heck, R. F.; Breslow, D. S. *J. Am. Chem. Soc.* **1962**, *84*, 2499−2502.

(8) Martin, J. T.; Baird, M. C. *Organometallics* **1983**, *2*, 1073−1078.

(9) Bartik, T.; Krummling, T.; Happ, B.; Sieker, A.; Marko, L.; Boese, R.; Ugo, R.; Zucchi, C.; Palyi, G. *Catal. Lett.* **1993**, *19*, 383−389.

(10) Kovacs, I.; Ungvary, F.; Marko, L. *Organometallics* **1986**, *5*, 209−215.

(11) Roe, D. C. *Organometallics* **1987**, *6*, 942−946.

(12) Pino, P.; Major, A.; Spindler, F.; Tannenbaum, R.; Bor, G.; Horvath, I. T. *J. Organomet. Chem.* **1991**, *417*, 65−76.

(13) Borovikov, M. S.; Kovacs, I.; Ungvary, F.; Sisak, A.; Marko, L. *Organometallics* **1992**, *11*, 1576−1579.

(14) Klingler, R. J.; Rathke, J. W. *J. Am. Chem. Soc.* **1994**, *116*, 4772−4785.

(15) Rathke, J. W.; Klinger, R. J.; Kramarz, K. W.; Woelk, K. *Prog. NMR Spectrosc.* **1997**, *30*, 209−253.

(16) Kramarz, K. W.; Klingler, R. J.; Fremgen, D. E.; Rathke, J. W. *Catal. Today* **1999**, *49*, 339−352.

(17) Rosi, L.; Piacenti, F.; Bianchi, M.; Frediani, P.; Salvini, A. *Eur. J. Inorg. Chem.* **1999**, 67−68.

industrially important homogeneous catalysis mechanisms for the carbonylation of organic feedstocks.

Migratory insertion has been extensively studied for model compounds such as $RMn(CO)_5$ and $CpFe(CO)_2R$ (Cp = η^5-C_5H_5, R = alky), e.g., eq 1.[18−21] For example, kinetics and
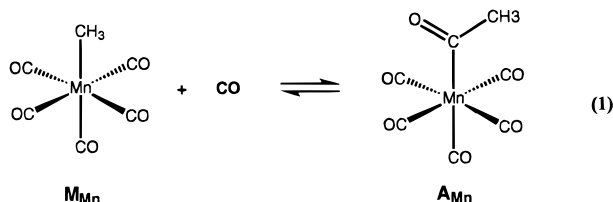
stereochemical studies of the reaction depicted in eq 1 concluded that this first involves migration of the methyl group from the metal to the cis CO ligand followed by trapping of the resulting "unsaturated" acyl intermediate $[CH_3C(O)Mn(CO)_4]$ (I_{Mn}) by CO.

Owing to their low steady state concentrations, such intermediates are difficult to observe directly under thermal reaction conditions. Therefore, this laboratory has utilized flash photolysis to probe the quantitative reactivities of possible intermediates in the migratory insertion reactions of model compounds noted in eq 1.[22−27] The method involves ligand photolabilization from an acyl complex such as **A** to generate non-steady-state concentrations of the coordinatively "unsaturated" reactive intermediate **I** (eq 2). Time-resolved infrared
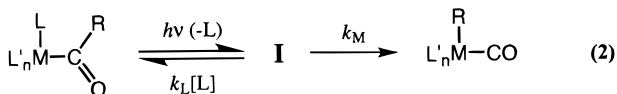
(TRIR) and time-resolved optical (TRO) detection[28−31] are then used to interrogate the spectra and reaction dynamics of **I**. The key reactions observed are the trapping of **I** by various ligands, including CO, to regenerate acyl complexes and the competing migration of the alkyl group from the acyl group of **I** to the metal center (the reverse of the insertion step). The dependence of the rate constants k_L and k_M obtained, respectively, for these two pathways with variables such as the nature of R and of the solvent provides valuable insight regarding the transition states for these pathways.

Described here are analogous investigations using the cobalt complex $CH_3C(O)Co(CO)_3(PPh_3)$ (A_{Co}) as a precursor. This

system clearly has an analogy and relevance to the industrially important, phosphine-modified cobalt carbonyl catalyst described above. These studies have been carried out using a high-pressure and variable temperature flow cell reactor[27] in order to examine the reactivity of presumed intermediates under a wide range of CO partial pressures (P_{CO}) and temperatures.

Experimental Section

Materials. The syntheses of $CH_3C(O)Co(CO)_3PPh_3$ and $CF_3C(O)Co(CO)_3PPh_3$ were carried out according to literature procedures.[7,32] Solvents were reagent grade and subjected to standard drying and distillation procedures.[33] Research grade carbon monoxide (99.995% purity from Spectra Gases) was used without further purification.

Solutions for TRIR Experiments. Solvents for flash photolysis experiments were deoxygenated by entrainment with argon or carbon monoxide or by repeated freeze−pump−thaw cycles. The concentrations of the cobalt solutions were typically 2−3 mM. This resulted in initial absorbances of 0.3−0.4 for the most intense of the terminal carbonyl stretches of the parent complex for a 0.5 mm path length. Solutions were prepared under various CO pressures (P_{CO}) and, after changes in P_{CO}, were stirred and given a minimum of 45 min to equilibrate. Concentrations of CO were calculated from published solubility data.[34,35] Both the step-scan and the single-frequency TRIR experiments were carried out using flowing sample solutions in order to minimize any complications arising from the accumulation and secondary photolysis of photoreaction products. The temperature of the solutions in the flow system and sample cell was regulated.

Step-Scan FTIR. The step-scan FTIR (BioRad FTS 60A/896) instrument at LANL has been described in previous publications.[36−38] In the configuration used here, a BioRad Fast TRS board controlled both the motion of the mirrors and data collection at a repetition rate of 10 Hz. The firing of the photolysis laser (355 nm output of a Nd:YAG laser) was synchronized to the mirror movement by a digital delay generator (Stanford Research Systems, model DG535) triggered by the TRS board. The spectral window of the instrument was 2250−1250 cm^{-1}, limited by a low-pass germanium optical filter at 2250 cm^{-1} and the CaF$_2$ windows of the IR cell at the lower frequency. The resolution of the transient difference spectra thus generated was 2 cm^{-1}.

The photolysis laser beam and the infrared output of the interferometer were overlapped and focused to a spot size of approximately 2 mm diameter onto a 0.5 mm path length CaF$_2$ IR cell (International Crystal Labs) through which the sample solutions of A_{Co} were flowed. The intensity of the transmitted IR beam was monitored by sampling the output of a mercury cadmium telluride (MCT) detector (Graseby 1710117, rise time 250 ns) and amplifier (Graseby DP-8000-4 amplifier, rise time of 1 μs) every 200 ns for 80 μs before and for 80 μs after the photolysis laser pulse at each mirror step. One transient was recorded for each interferometer step, so multiple scans were averaged to improve the signal-to-noise (s/n) ratio. Thus, an array of interferograms with respect to time was constructed during each step-scan experiment from which were extracted transient difference spectra for different times. Transient difference spectra were generated using the expression $\Delta A(t,\nu) = -\log(I(t,\nu)/I_0(\nu))$ where $I_0(\nu)$ is the average transmitted intensity before the laser pulse at frequency ν.

Unless otherwise noted, the solvent used in the step-scan FTIR experiments was deuterated benzene (Aldrich). Carbon monoxide (Matheson, scrubbed for both oxygen and water) was bubbled through

(18) Atwood, J. D. *Inorganic and organometallic reaction mechanisms*; Brooks/Cole Publishing Co.: Monterey, CA, 1985.
(19) Cavell, K. J. *Coord. Chem. Rev.* **1996**, *155*, 209−243.
(20) Collman, J. P.; Hegedus, L. S.; Norton, J. R.; Finke, R. G. *Principles and applications of organotransition metal chemistry*; University Science Books: Mill Valley, CA, 1987.
(21) Jordon, R. B. *Reaction Mechanisms of Inorganic and Organometallic Systems*, 2nd ed.; Oxford University Press: New York, 1998.
(22) Boese, W. T.; Ford, P. C. *Organometallics* **1994**, *13*, 3525−3531.
(23) Boese, W. T.; Ford, P. C. *J. Am. Chem. Soc.* **1995**, *117*, 8381−8391.
(24) McFarlane, K. L.; Ford, P. C. *Organometallics* **1998**, *17*, 1166−1168.
(25) McFarlane, K. L.; Lee, B.; Fu, W. F.; van Eldik, R.; Ford, P. C. *Organometallics* **1998**, *17*, 1826−1834.
(26) Belt, S. T.; Ryba, D. W.; Ford, P. C. *J. Am. Chem. Soc.* **1991**, *113*, 9524−9528.
(27) Massick, S. M.; Ford, P. C. *Organometallics* **1999**, *18*, 4362−4366.
(28) DiBenedetto, J. A.; Ryba, D. W.; Ford, P. C. *Inorg. Chem.* **1989**, *28*, 3503−3507.
(29) Ford, P. C.; DiBenedetto, J. A.; Ryba, D. W.; Belt, S. T. *SPIE Proc.* **1992**, *1636*, 9−16.
(30) Ford, P. C.; Bridgewater, J. S.; Lee, B. *Photochem. Photobiol.* **1997**, *65*, 57−64.
(31) Ford, P. C.; Bridgewater, J. S.; Massick, S.; Marhenke, J. *Catal. Today* **1999**, *49*, 419−430.

(32) Lindner, E.; Zipper, M. *Chem. Ber.* **1974**, *107*, 1444−1455.
(33) Riddick, J. A.; Bunger, W. B.; Sakano, T. K. *Organic Solvents Physical Properties and Methods of Purification*, 4th ed.; John Wiley & Sons: New York, 1986; Vol. II.
(34) *IUPAC Solubility Data Series: Carbon Monoxide*; Pergamon Press: Oxford, 1990; Vol. 43.
(35) Payne, M. W.; Leussing, D. L.; Shore, S. G. *J. Am. Chem. Soc.* **1987**, *87*, 617−618.
(36) Schoonover, J. R.; Strouse, G. F. *Chem. Rev.* **1998**, *98*, 1335−1355.
(37) Schoonover, J. R.; Strouse, G. F.; Dyer, R. B.; Bates, W. D.; Chen, P. Y.; Meyer, T. J. *Inorg. Chem.* **1996**, *35*, 273−274.
(38) Schoonover, J. R.; Strouse, G. F.; Omberg, K. M.; Dyer, R. B. *Comments Inorg. Chem.* **1996**, *18*, 165−188.
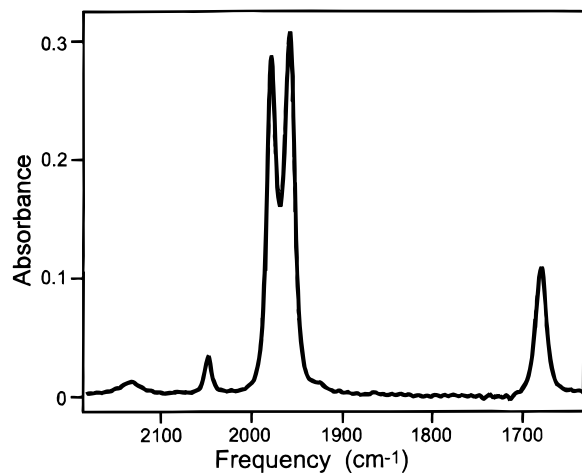
Figure 1. Infrared spectrum of a 2.14 mM solution of the parent complex $CH_3C(O)Co(CO)_3PPh_3$ ($\mathbf{A_{Co}}$) in deuterated benzene equilibrated with 1 atm of carbon monoxide. The peak positions are 1680 cm^{-1} for the acyl ν_{CO}, 1959, 1979, 2048 cm^{-1} for the terminal ν_{CO}, and 2131 cm^{-1} for free CO in solution.

Figure 2. Infrared transient difference spectra of $CH_3C(O)Co(CO)_3$-PPh$_3$ ($\mathbf{A_{Co}}$) in C_6D_6 recorded after 355 nm flash photolysis. The overlay of spectra indicates 5 μs intervals ranging from 0 to 40 μs following the laser pulse.

the solutions for 20 min. The solutions were then transferred to a 50 mL gastight syringe (Hamilton) and attached to a flow system consisting of the CaF$_2$ IR cell followed by another 50 mL gastight syringe. Two syringe pumps were alternately used to cycle the solution from syringe to syringe at a rate of approximately 2 mL/min during the course of the experiment. Typically, at least four scans were averaged to obtain a satisfactory s/n ratio.

Single-Frequency Time-Resolved Infrared Studies. The apparatus for TRIR studies at UCSB has been described previously.[28,30] In the present configuration, the probe source consists of four lead-salt diode lasers mounted on a Spectra Physics/Laser Analytics model SP5731 laser head and a CVI Digikrom model 240 monochromator. This configuration provides a tunable infrared probe laser source with frequencies between 2200 and 1500 cm^{-1}. The probe laser beam was focused to a 7 mm diameter spot and overlapped at the plane of the sample cell with the 355 nm pump pulse from a Lumonics HY600 Nd:YAG laser. The transmitted intensity of the infrared probe beam was focused to fill the 1 mm^2 active area of a Fermionics model PV-8-1 photovoltaic Hg/Cd/Te detector. A Fermionics model PVA 500-50 preamplifier increased the signal from the detector 20-fold prior to digitization by a LeCroy 9400 oscilloscope at a rate of 100 MHz.

A recently constructed high-pressure and variable-temperature (HPVT) flow system[27] was used in these studies. This system allows for the equilibration of sample solutions in a modified Parr bomb with gas pressures up to 100 atm and temperatures up to 150 °C. During the photolysis experiments, sample solutions of a known CO concentration and temperature were allowed to flow from the Parr Bomb through a high-pressure IR cell modified on the basis of modifications to a published design[39] of a low-pressure reservoir. The jacketed transfer lines and HPVT IR cell were all maintained at the same temperature and pressure as the Parr bomb reservoir.

Results

The infrared absorption spectrum of the parent complex $CH_3C(O)Co(CO)_3PPh_3$ ($\mathbf{A_{Co}}$) is shown in Figure 1. This is consistent with a trigonal bipyramidal arrangement of the five ligands with the three carbonyls in the equatorial plane and the acyl and phosphine groups in the axial sites.[40,4140,41] The A$_1$ and E modes expected for the terminal carbonyl stretches in local C_{3v} symmetry are observed in benzene-d_6 at ν_{CO} = 2048,
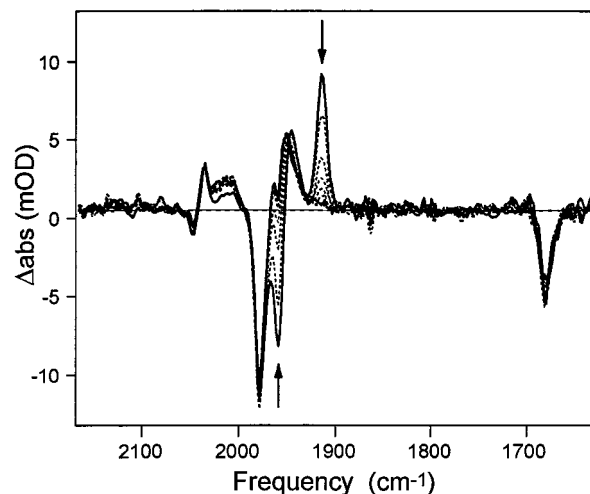
1979, and 1959 cm^{-1} with the degeneracy of the lower energy E mode split because of a lowering of the symmetry by the acyl group. The weaker acyl carbonyl stretch is also observable at ν_{CO} = 1680 cm^{-1}.

Step-Scan FTIR Studies. These experiments at LANL provided a clear insight into the events following the 355 nm photolysis of the parent complex $\mathbf{A_{Co}}$. The spectra from sequential 5 μs intervals following the photolysis pulse are shown in Figure 2. This clearly depicts the prompt bleach of the parent terminal ν_{CO} absorbances at 2048, 1979, and 1959 cm^{-1} characteristic of $\mathbf{A_{Co}}$ and the prompt formation and decay of a transient species $\mathbf{I_{Co}}$ with a strong isolated absorbance at 1915 cm^{-1}. The bleach of the acyl ν_{CO} band at 1680 cm^{-1} was also seen. However, the interpretation of the temporal absorbance changes between 1965 and 1940 cm^{-1} is less clear. The bleach of the terminal ν_{CO} of $\mathbf{A_{Co}}$ at 1959 cm^{-1} and an apparent prompt absorbance at 1946 cm^{-1} attributable to $\mathbf{I_{Co}}$ overlap with other absorbance changes attributed to formation of a "permanent" photoproduct.[42]

The temporal response of the bleach of $\mathbf{A_{Co}}$ at 1979 cm^{-1} for the transient absorbance of the intermediate $\mathbf{I_{Co}}$ at 1915 cm^{-1} and for the product formation at 1958 cm^{-1} are shown in curves a, b, and c of Figure 3, respectively. The behavior of the product absorbance at 1958 cm^{-1} (Figure 3c) merits some comment because this region overlaps directly with absorbance changes arising from $\mathbf{A_{Co}}$. The baseline reference for the temporal transient absorption traces is normally defined by a selecting a frequency interval in a spectral region where there are no observed absorbance changes. However, in this instance a correction for the overlap of the bleach of $\mathbf{A_{Co}}$ at 1959 cm^{-1} with the product absorbance at 1958 cm^{-1} was approximated by selecting a frequency interval for the baseline reference that includes the bleach of $\mathbf{A_{Co}}$ at 1979 cm^{-1} to account for both the bleach and regeneration of $\mathbf{A_{Co}}$. The frequency intervals for the product and baseline regions were 1960–1957 and 1980.5–1977.5 cm^{-1}, respectively. (Alternatively, a similar kinetic trace with the same rate of exponential rise but much lower amplitude could be obtained by selecting a narrow frequency interval centered about 1953 cm^{-1}.) The kinetic trace of product

(39) Noack, K. *Spectrochim. Acta* **1968**, *43*, 1024–1026.
(40) Kovacs, I.; Ungvary, F. *Coord. Chem. Rev.* **1997**, *161*, 1–32.
(41) Somlyai-Haasz, J.; Haasz, F.; Galamb, V.; Benedetti, A.; Zucchi, C.; Palyi, G.; Krummling, T.; Happ, B.; Bartik, T. *Organometallics* **1991**, *10*, 205–217.

(42) Given that over a much longer time scale this photoproduct reacts with CO to regenerate $\mathbf{A_{Co}}$, the term "permanent" refers only to spectral changes on the time scale of the TRIR experiments.
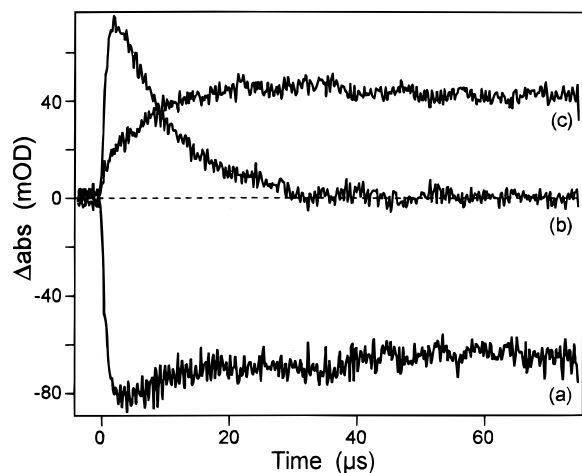
Figure 3. Absorption changes following 355 nm flash photolysis of $CH_3C(O)Co(CO)_3PPh_3$ (A_{Co}) in C_6D_6 monitored at (a) 1979 cm^{-1} corresponding to the bleach of the parent complex A_{Co}, (b) 1915 cm^{-1} due to the absorption of the transient intermediate $CH_3C(O)Co(CO)_2$-PPh_3 (I_{Co}), and (c) 1958 cm^{-1} showing the formation of the methyl cobalt complex $CH_3Co(CO)_3PPh_3$ (M_{Co}) (generated by setting a baseline region about 1979 cm^{-1} to correct for the parent bleach at 1959 cm^{-1}).
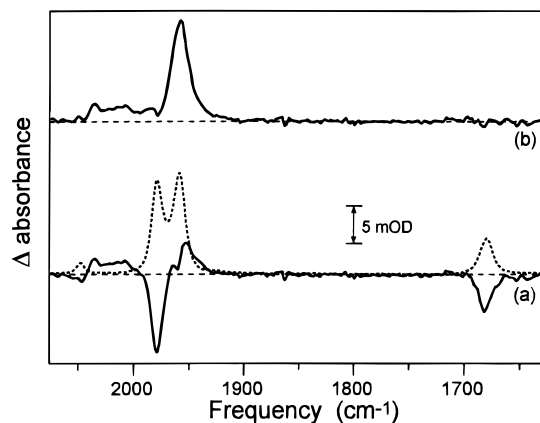

Figure 4. (a) Transient difference spectrum extracted from the time interval 40−80 μs following the 355 nm photolysis of $CH_3C(O)Co(CO)_3$-PPh_3 (A_{Co}) in C_6D_6, [CO] ≅ 5mM, and the infrared spectrum of A_{Co}. (b) Sum of difference spectrum and enough of the parent spectrum to equal the bleach at 1680 cm^{-1}.

formation at 1958 cm^{-1} fits well to an exponential rise with an observed rate constant (k_{obs}) of approximately 1.3×10^5 s^{-1}. This value is in agreement with the k_{obs} (1.2×10^5 s^{-1}) obtained from an exponential fit of the decay of I_{Co} at 1915 cm^{-1} (Figure 3b), so it is reasonable to assume that I_{Co} reacts directly to form this photoproduct. Also of note, under these conditions ($P_{CO} \cong$ 0.76 atm) the regeneration of A_{Co} on this time scale is at most quite modest (Figure 3a).

Since the decay of I_{Co} is essentially complete by 40 μs, it is possible to characterize the "permanent" product of the 355 nm photolysis of A_{Co} by extracting a difference spectra for the 40−80 μs after photolysis (Figure 4a). The components of the (40−80 μs) difference spectrum are the bleach of the parent spectrum and the absorbance spectra associated with the photoproduct(s). The latter can be generated by adding a weighted amount of the A_{Co} spectrum (Figure 4a) to the extracted difference spectrum. Since the acetyl group ν_{CO} at 1680 cm^{-1} does not overlap with other bands, the amplitude of the absorbance change at this frequency provides a convenient measure of the weighting factor. The resulting spectrum (Figure 4b) appears to be that of the expected methyl complex[43] $CH_3Co(CO)_3PPh_3$
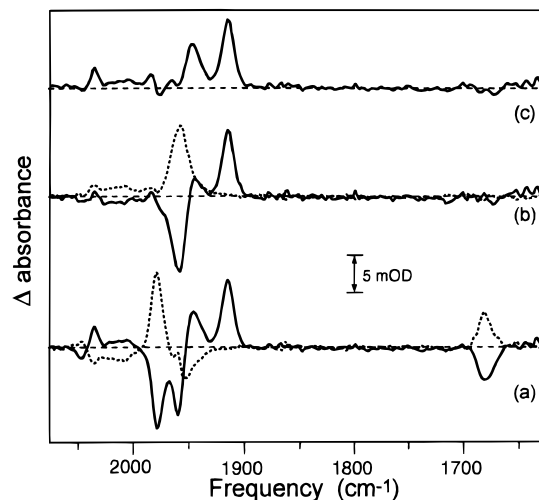
Figure 5. (a) Transient difference spectrum extracted from the first 1.5 μs following 355 nm photolysis of $CH_3C(O)Co(CO)_3PPh_3$ (A_{Co}) in C_6D_6 (solid line) and the negative of the transient difference spectrum for the time period from 40 to 80 μs (dashed line). (b) Resultant spectrum from the addition of the spectra in (a) (solid line) and the weighted product spectrum of $CH_3Co(CO)_3PPh_3$ (M_{Co}) as shown in Figure 4b (dashed line). (c) Resultant spectrum of the intermediate formed during the first 1.5 μs following the photolysis laser pulse.

Scheme 2
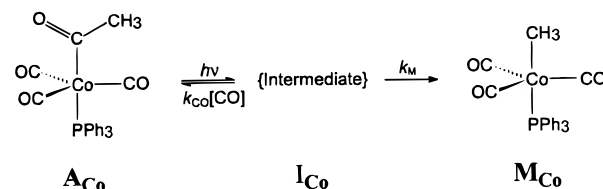
(M_{Co}). However, there is a broad weak feature between 2030 and 1990 cm^{-1} possibly attributable to solvent heating because benzene-d_6 has some absorbance in this region. These results are consistent with the scenario illustrated in Scheme 2; photolysis of the acetyl complex A_{Co} gives a reactive intermediate I_{Co} that reacts further to give M_{Co} or to re-form A_{Co}.

The spectrum of I_{Co} can be generated by a similar analysis of the difference spectrum extracted from the first 1.5 μs after the pump laser pulse (Figure 5a). This (0−1.5 μs) difference spectrum was corrected for "permanent" absorbance changes such as the bleach of A_{Co} or product formation after the first 1.5 μs by subtracting the difference spectrum for the final 40 μs (Figure 4a) weighted to compensate for the bleach of the acetyl group at 1680 cm^{-1}. However, as can be seen in Figure 5b, some of the M_{Co} has already formed during the first 1.5 μs. Thus, addition of a weighted spectrum of M_{Co} (Figure 4b) from Figure 5b generates a spectrum with absorbance changes at 1915, 1947, 2035, and possibly 1983 cm^{-1}. The absorbance of I_{Co} at 1915 cm^{-1} provides an excellent region of the IR for monitoring the kinetics of the intermediate I_{Co} free from overlap of absorbance changes from either parent A_{Co} or photoproduct M_{Co}.

Single-Frequency TRIR Studies The single-frequency detection methodology of the TRIR apparatus at UCSB is especially well-suited for accurate kinetics measurements. Furthermore, the HPVT flow system[27] allows the laser photolysis experiments to be conducted on sample solutions of A_{Co} equilibrated under a wide range of P_{CO} and temperature. In the present case, the range of P_{CO} employed was from 0 to 11 atm

(43) Hieber, W.; Lindner, E. *Chem. Ber.* **1961**, *94*, 1417−1425.
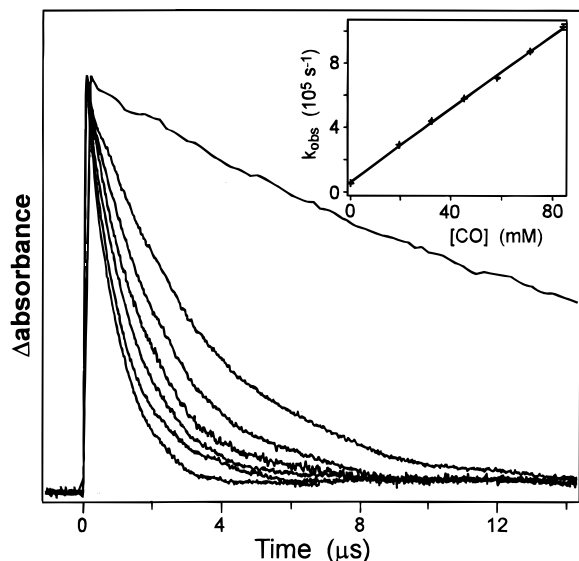
Figure 6. Overlay of transient absorptions of $CH_3C(O)Co(CO)_2PPh_3$ (I_{Co}) at 1915 cm^{-1} following 355 nm flash photolysis of $CH_3C(O)Co(CO)_3PPh_3$ (A_{Co}) in benzene at 25 °C and [CO] = 0, 20, 32, 45, 58, 71, and 84 mM from top to bottom, respectively. The initial absorbance change of the individual traces were normalized to unity to better illustrate the change in the decay rate. The inset graph is a plot of the observed rate constant, k_{obs}, obtained from single-exponential fits vs [CO] for the same data.
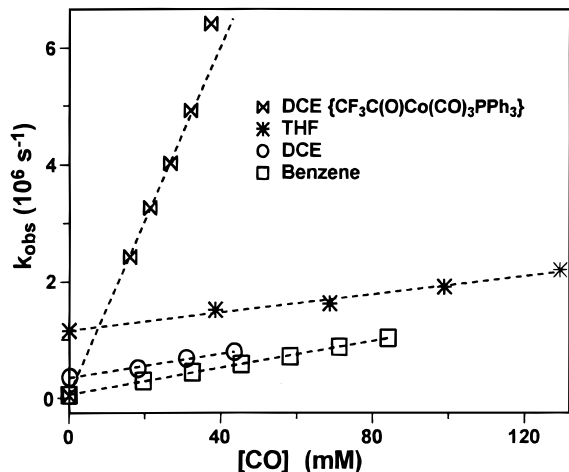
Figure 7. Plot of the observed rate constant k_{obs} vs the CO concentration for benzene, dichloroethane (DCE), tetrahydrofuran (THF) as indicated for the decay of the transient intermediate $CH_3C(O)Co(CO)_2$-PPh_3 (I_{Co}). Also included is the plot of k_{obs} vs [CO] for the trifluoroacetylcobalt complex (I_F).

while T was varied from 25 to 45 °C. Variation of P_{CO} over this range was necessary to determine the reactivities of I_{Co} toward CO to re-form A_{Co}, while variation of T provides the opportunity to measure the activation parameters $\Delta H^{\ddagger}$ and $\Delta S^{\ddagger}$ for both the k_M and k_{CO} pathways.

Shown in Figure 6 are the curves representing the decay of I_{Co} monitored at 1915 cm^{-1} in 25 °C benzene solutions equilibrated with various P_{CO} ranging from 0 to 11.3 atm. These P_{CO} values correspond to CO concentrations from 0 to 84 mM.[33,34] The curves can be fit as single-exponential decays, the rates of which increase linearly with [CO] (Figure 7). This is consistent with the observation that on the microsecond to millisecond time scale the bleaches of the parent complex at 1980 and 1679 cm^{-1} (Figure 8) both recover substantially in the presence of high [CO] but very little for solutions equilibrated under ~0.76 atm CO (Figure 3). The decay of I_{Co} as a
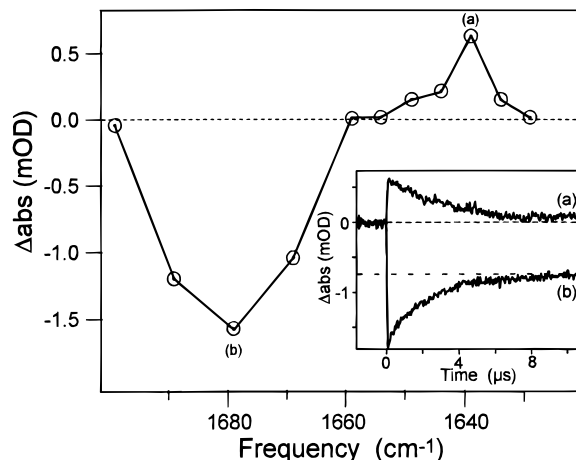
Figure 8. Transient difference spectrum in the acyl stretching region for the initial 0.5 ms following the photolysis of A_{Co} in benzene at 25 °C and [CO] = 0.0324 M. Transient absorptions were collected at single frequencies in a point-by-point fashion. The inset plot depicts the change in absorption at 1639 cm^{-1} (a) and 1679 cm^{-1} (b). The temporal trace (a) is an average of three separate 80 shot acquisitions and that of (b) is a single 80 shot acquisition.

Table 1. Rate Constants for Methyl Migration, k_M, and for Reaction with CO, k_{CO}, Following 355 nm Photolysis of $CH_3C(O)Co(CO)_3PPh_3$ and $CF_3C(O)Co(CO)_3PPh_3$ in Various Solvents at 25 °C

solvent	k_M (10^5 s^{-1})	k_{CO} (10^6 M^{-1} s^{-1})
	$CH_3C(O)Co(CO)_3PPh_3$	
tetrahydrofuran	12 ± 0.4	7.8 ± 0.5
benzene	0.62 ± 0.07	11.4 ± 0.1
dichloromethane	1.9 ± 0.2	16 ± 1
dichloroethane	3.5 ± 0.2	10 ± 0.8
	$CF_3C(O)Co(CO)_3PPh_3$	
dichloroethane	0.46 ± 0.01	150 ± 6

function of [CO] can be modeled by a simple competition between two available reaction paths: a unimolecular methyl migration with the associated rate k_M to form M_{Co}; and a bimolecular reaction with CO with the associated rate k_{CO} to re-form A_{Co} (Scheme 2), with the observed rate constant k_{obs} = $k_{CO}[CO] + k_M$. Accordingly, a plot of k_{obs} vs [CO] is linear (Figure 6 inset) with the slope k_{CO} = 1.14 (± 0.01) $\times 10^7$ M^{-1} s^{-1} and the intercept k_M = 6.2 (± 0.7) $\times 10^4$ s^{-1}.

The reactivity of I_{Co} generated by flash photolysis of A_{Co} was also investigated in 1,2-dichloroethane (DCE), dicholoro-methane (CH$_2$Cl$_2$), and tetrahydrofuran (THF) solutions at 25 °C. In each case plots of k_{obs} vs [CO] were linear with nonzero intercepts (Figure 7). The k_{CO} and k_M values so obtained are summarized in Table 1. Notably, there is little variation in k_{CO} with the nature of the solvent; the highest value of 1.6 (± 0.1) $\times 10^7$ M^{-1} s^{-1} in CH$_2$Cl$_2$ is only a factor of 2 higher than the lowest in THF. The transient spectra also display little change in ν_{CO} values found for I_{Co} of 1915 (± 2) cm^{-1}, 1914 (± 2) cm^{-1}, and 1913 (± 4) cm^{-1} in deuterated benzene, DCE, and THF, respectively. These were determined both by the step-scan FTIR technique (DCE and benzene) and from the point-by-point single-frequency TRIR method (THF).

In contrast to the behavior of k_{CO}, the rate constant for methyl migration k_M is more sensitive to the nature of the solvent (Table 1). For example, the value found in THF (k_M = 12 (± 0.4) $\times 10^5$ s^{-1}) is almost 20 times faster than that measured in benzene (k_M = 6.2 (± 0.7) $\times 10^4$ s^{-1}) at 25 °C. The values obtained for k_M in the less donating solvents benzene, CH$_2$Cl$_2$, and DCE follow the order of the dielectric constants (ϵ_r = 2.3, 8.9, 10.4,

Table 2. Rate Constants and Activation Parameters for Methyl Migration, k_M, and for Reaction with CO, k_{CO}, Following 355 nm Photolysis of $CH_3C(O)Co(CO)_3PPh_3$ in Benzene

temp (°C)	k_M (10^4 s^{-1})	k_{CO} (10^7 M^{-1} s^{-1})
25	6.2 (±0.7)	1.14 (±0.01)
30	7.6 (±0.5)	1.19 (±0.01)
35	10.5 (±0.9)	1.26 (±0.02)
40	13.5 (±0.6)	1.34 (±0.01)
45	18.0 (±0.8)	1.40 (±0.02)
$\Delta H^{\ddagger}$ (kJ mol^{-1})	40 (±2)	5.7 (±0.4)
$\Delta S^{\ddagger}$ (J mol^{-1} K^{-1})	−19 (±5)	−91 (±12)

respectively).[33] Such an observation might suggest that the solvent effect on the methyl migration pathway is due to stabilization of a transition state for the k_M pathway more polar than I_{Co}. However, the k_M value measured in THF (ϵ_r = 7.6) is anomalous and suggests that (at least in this case) the solvent may be acting in a more intimate manner, perhaps as a donor via the THF oxygen.

To determine the activation parameters $\Delta H^{\ddagger}$ and $\Delta S^{\ddagger}$ for the two competitive pathways, k_{CO} and k_M, the kinetics for the decay of I_{Co} were examined by TRIR spectroscopy in benzene over the temperature range 25−45 °C in 5 °C increments. These data are summarized in Table 2. Plots of k_{obs} vs [CO] are linear at each temperature, and both k_{CO} and k_M increase with T. However, the temperature sensitivity of k_{CO} is slight (indicative of a small enthalpic barrier), while that of k_M is much larger. From a linear least-squares fit of an Eyring plot (Figure S-2 of Supporting Information) for k_{CO} the enthalpy of activation $\Delta H^{\ddagger}_{CO}$ and entropy of activation $\Delta S^{\ddagger}_{CO}$ were determined to be 5.7 ± 0.4 kJ mol^{-1} and −91 ± 12 J mol^{-1} K^{-1}, respectively. An Eyring plot for k_M gave $\Delta H^{\ddagger}_M$ and $\Delta S^{\ddagger}_M$ values for the methyl migration pathway of 40 ± 2 kJ mol^{-1} and −19 ± 5 J mol^{-1} K^{-1}, respectively.

Although the transient difference spectra obtained from the step-scan FTIR experiments in the solvents C_6D_6 and DCE did not show any absorbances in the acyl region that could be convincingly related to I_{Co}, the TRIR photolysis experiments using the single-frequency probe source were successful in this regard. Shown in Figure 8 is a transient difference spectrum (collected point by point) of the acyl region averaged over a 0.5 μs interval immediately following the flash photolysis of A_{Co} in benzene. Prompt bleaching of the parent acyl ν_{CO} at 1680 cm^{-1} is seen as well as the formation of a new absorbance at 1639 cm^{-1}. The inset plot in Figure 8 shows the time evolution of the signals at 1680 and at 1639 cm^{-1} for TRIR experiments carried out with P_{CO} = 4.4 atm. Despite the weakness of the acyl signal, the regeneration of A_{Co} (k_{obs} = 4.6 (±0.1) × 10^5 s^{-1}) nearly matches the k_{obs} value of 4.4 (±0.14) × 10^5 s^{-1} calculated for I_{Co} in 25 °C benzene from the data in Table 1 for 32.4 mM CO. The even weaker decay of the absorbance change at 1639 cm^{-1} (k_{obs} = 3.5 (±0.4) × 10^5 s^{-1}) is also in reasonable agreement. These observations are taken as evidence that the absorbances at 1639, 1915, and 1947 cm^{-1} are all characteristic of a single species I_{Co} and that loss of a carbonyl ligand from A_{Co} shifts the acyl carbonyl stretching frequency 41 (±2) cm^{-1} lower in energy for I_{Co}.

$CF_3C(O)Co(CO)_3PPh_3$. To investigate the role that the acetyl group plays in the stabilization of I_{Co}, photolysis experiments on the trifluoroacetylcobalt derivative $CF_3C(O)Co(CO)_3PPh_3$ (A_F) were performed. The infrared spectrum of A_F displays ν_{CO} at 2067(w), 2012(s), 1986(s), and 1666(m) cm^{-1}, similar to the spectrum of A_{Co} but with ν_{CO} bands generally shifted to higher energy. Flash photolysis of A_F (355 nm) in DCE at 25 °C leads to prompt bleaching of the parent ν_{CO} absorption and generates

a transient species with a ν_{CO} at 1935 cm^{-1} corresponding to the production of a transient intermediate presumably, $CF_3C(O)Co(CO)_2PPh_3$ (I_F). A transient absorbance for the acyl ν_{CO} was also observed to lower energy for I_F at 1650 cm^{-1} shifted only 16 ± 3 cm^{-1} from the acyl ν_{CO} of A_F.

The temporal behavior of the transient absorbances attributed to I_F also fit well to single-exponential decays with k_{obs} values strongly dependent on [CO]. The plot of k_{obs} vs [CO] for I_F proved to be linear with the slope k_{CO}(25 °C) = 1.5 (±0.06) × 10^8 M^{-1} s^{-1} and a nonzero intercept k_M(25 °C) = 4.6 (±0.1) × 10^4 s^{-1} (Table 1). Notably, k_M is an order of magnitude smaller and k_{CO} is 15 times larger than the respective values for I_{Co} in DCE.

Discussion

The 355 nm flash photolysis of A_{Co} leads to CO dissociation and prompt formation of the "unsaturated" acetyl complex $CH_3C(O)Co(CO)_2PPh_3$, I_{CO}. This reacts with CO (k_{CO}) to reform the initial complex in competition with methyl group migration from the acyl group to the cobalt (k_M), in steps analogous to steps d and e of Scheme 1, respectively. The transient IR spectra are consistent with I_{Co} being the primary photoproduct, although manipulations of the step-scan spectral data leave some doubt as to whether the minor product $CH_3C(O)Co(CO)_3$ (I'_{Co}) is formed by phosphine photodissociation. The latter should have higher frequency ν_{CO} bands consistent with the observation of weaker bands at 2035 and possibly 1983 cm^{-1} in the step-scan spectra (Figure 5c). Earlier photolysis studies by Sweany[44] of $CH_3C(O)Co(CO)_4$ (A'_{Co}) in argon matrices demonstrated the formation of a species formulated as I'_{Co}, which displayed bands at 2081(m), 2008(s), 1977(s), and 1686 (w) cm^{-1}, so it is possible that the two stronger bands of these correspond to the unassigned weak bands seen in Figure 5c. However, the absorbance at 1983 cm^{-1} is close to the A_{Co} band at 1979 cm^{-1} and its intensity varies depending on how the bleach of the latter band is weighted in the difference spectrum,[45] while that at 2035 cm^{-1} overlaps directly with the symmetric ν_{CO} of M_{Co}. This peak appears to be invariant to the manner by which the transient spectra are generated and may indicate that some M_{Co} formed promptly during the flash photolysis of A_{Co}. Indeed, regeneration of the A_{Co} band at 1979 cm^{-1} was observed to be consistently somewhat less than predicted by ratios of k_M and k_{CO}[CO]. Similar prompt (minor) formation of the methyl complex was observed in the flash photolysis of $CH_3C(O)Mn(CO)_5$, A_{Mn}.[22] Regardless of these possible minor pathways, the dynamics of I_{Co} decay, A_{Co} reformation, and M_{Co} formation are all shown to be closely coupled and unaffected by the possible formation of a minor secondary product, so the ensuing discussion will not be further concerned with this issue.

What is the Structure of I_{Co}? The step-scan FTIR spectrum recorded during the first 1.5 μs following photolysis of A_{Co} in

(44) Sweany, R. L. *Organometallics* **1988**, *8*, 175−179.
(45) Mixing in a weighted spectrum of A_{Co} instead of subtracting the difference spectrum from the time interval 40−80 μs results in a somewhat stronger absorbance at 1983 cm^{-1}. (In either case, an additional correction is required to compensate for the amount of the final product M_{Co} formed during the first 1.5 μs, and this spectrum of M_{Co} is itself generated by addition of the spectrum of A_{Co} (only 3−4%) to the 40−80 μs difference spectrum.) Notably, the absorbance of the peak of A_{Co} at 1979 cm^{-1} is 0.3 (50% Δ transmittance) in the spectrum used in these subtractions and any nonlinear detector response could affect line shapes to the extent that would result in poor subtractions with the weak transient spectra showing absorbance changes of only 0.003 (0.7% Δ transmittance) at 1983 cm^{-1}. This latter consideration gives greater confidence to the transient spectra mixed with the least amount of the spectrum of A_{Co}.

Scheme 3
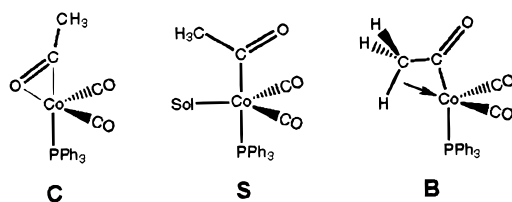
benzene-d_6 (Figure 5c) displays the ν_{CO} peaks at 1947 and 1915 cm^{-1} with the expected shift to lower energy of the ν_{CO} of the remaining terminal CO ligands upon loss of one CO. Interpretation of the spectra and kinetics of the "unsaturated" species $\mathbf{I_{Co}}$ can be discussed in terms of three potential structures, the cyclic η^2-acyl complex **C**, the solvent-stabilized species **S**, or the bidentate β-agostic complex **B**. In each structure the vacant coordination site is stabilized via interaction with a Lewis base, i.e., interaction with the lone pairs of the carbonyl oxygen or with a C−H bonding electron pair of the acyl methyl or with a C−H or lone pair from the solvent.

It is evident from Table 1 that the rate constant k_{CO} for the reaction of $\mathbf{I_{CO}}$ with CO is relatively insensitive to the solvent medium; k_{CO} in THF is only a factor of 2 less than in CH$_2$Cl$_2$ and about 30% less than in benzene. Since the rates of CO reaction with various solventometal carbonyl species such as Cr(CO)$_5$(Sol)[46] and CH$_3$Mn(CO)$_4$(Sol)[22] are markedly dependent on the nature of Sol, the behavior of $\mathbf{I_{Co}}$ argues against this species having the **S** configuration in the four solvents discussed here. Instead it is likely that the site left open by CO photodissociation is stabilized by coordination to the acetyl group. Such coordination may be via η^2-binding of the acyl carbonyl as in **C** or by an agostic interaction with a methyl C−H as in **B**. This conclusion is reinforced by the insensitivity of the principal ν_{CO} band of $\mathbf{I_{Co}}$ at ∼1915 cm^{-1} to the same solvents.

In accord with the interpretation that $\mathbf{I_{CO}}$ is not the solvento complex **S**, it is notable that the entropies of activation for the "unimolecular" acetyl-to-cobalt methyl migration ($\Delta S^{\ddagger}_M = -19$ J mol^{-1} K^{-1}) and the bimolecular CO addition ($\Delta S^{\ddagger}_{CO} = -91$ J mol^{-1} K^{-1}) determined in benzene are both negative. This would further indicate that, in this medium, neither pathway is dominated kinetically by a step involving solvent dissociation.

These observations and conclusions can be compared to an earlier TRIR study here of the reaction dynamics and spectra of the analogous manganese intermediate CH$_3$C(O)Mn(CO)$_4$, $\mathbf{I_{Mn}}$.[22,23] That system also showed little variation of k_{CO} from various weak donor solvents ranging from perfluoromethylcyclohexane to CH$_2$Cl$_2$, and it was argued that $\mathbf{I_{Mn}}$ has the η^2-acyl configuration **C** in these media. Consistent with this suggestion was the shift of the acyl ν_{CO} from 1661 cm^{-1} for $\mathbf{A_{Mn}}$ to 1607 cm^{-1} for $\mathbf{I_{Mn}}$ in alkane solutions, although it should be noted that replacing CO with nearly any ligand would be expected to shift this band to lower frequency. However, in THF, k_{CO} was more than an order of magnitude smaller[47] and the terminal ν_{CO} bands for $\mathbf{I_{Mn}}$ exhibited a clear shift to lower energy, leading to the interpretation that, *unlike* $\mathbf{I_{Co}}$, $\mathbf{I_{Mn}}$ has the solvento configuration in THF.

However, the above data do not differentiate between the structures **C** and **B** for $\mathbf{I_{Co}}$, since both involve intramolecular stabilization of the vacant coordination site by the acetyl ligand. The absorbance changes in the acyl region clearly show a ν_{CO} band at 1639 cm^{-1} attributed to $\mathbf{I_{Co}}$ shifted 41 cm^{-1} to lower frequency and with a relative intensity no more than a third that of the acyl band for $\mathbf{A_{Co}}$ at 1680 cm^{-1}. In Sweany's study[44] of CH$_3$C(O)Co(CO)$_4$ ($\mathbf{A'_{Co}}$) in argon matrices, 310 nm photolysis produced the unsaturated complex $\mathbf{I'_{Co}}$ with an acyl band at 1686 cm^{-1}, a comparable 38 cm^{-1} shift from that for $\mathbf{A'_{Co}}$. Under these conditions $\mathbf{I'_{Co}}$ was remarkably stable even in the presence of CO and H$_2$, whereas the methyl and hydride analogues CH$_3$Co(CO)$_3$ and HCo(CO)$_3$ (from photolysis of the methyl and hydridotetracarbonylcobalt complexes,[48] respectively) both react readily with CO and H$_2$. Furthermore, the relative intensity of the acyl ν_{CO} observed for $\mathbf{I'_{Co}}$ was only 30% that of the parent complex $\mathbf{A'_{Co}}$. Clearly, the reactivity patterns and spectral properties for $\mathbf{I_{Co}}$ and $\mathbf{I'_{Co}}$ are sufficiently similar that it is likely that their structures are also similar.

Sweany has attributed the diminished intensity of the acyl ν_{CO} band to a cyclic η^2-conformation for the acyl group of $\mathbf{I'_{Co}}$, resulting in weakening of the dipole moment derivative of the C−O stretch due to opposing changes in the dipoles of the Co−O and Co−C bonds in **C′**. This assignment draws support from density functional calculations on reactive intermediates of the unmodified cobalt-catalyzed hydroformylation cycle by Ziegler et al.,[49−51] which predict the η^2-acyl structure (**C′**) for CH$_3$C(O)Co(CO)$_3$ as the most stable conformation for $\mathbf{I'_{Co}}$. Two η^2-conformations were predicted, one with the acyl group in the equatorial site. The other with the acyl carbon in the axial site and the oxygen pointing toward the equatorial site as shown in **C** is predicted to be the more stable.[50] The **C′** conformations were predicted to be lower in energy than the corresponding agostic **B′** conformations by a minimum of 16 kJ mol^{-1} in each case.

There are now numerous examples of stable η^2-acyl complexes that have been structurally characterized.[52,53] These generally show lower acyl ν_{CO} frequencies than displayed by either $\mathbf{I_{Co}}$ or $\mathbf{I'_{Co}}$. However, a more important comparison would be the shift in the acyl band when a terminal CO and the resulting vacancy is occupied by an η^1-acyl rearranging to η^2-coordination. For example,[52] the iron(II) complex Fe(η^1-C(O)CH$_2$CMe$_3$)Br(CO)$_2$dippe (dippe is 1,2-bis(diisopropylphosphino)ethane) displays terminal ν_{CO} bands at 2004 and 1959 cm^{-1} and an acyl ν_{CO} absorption at 1634 cm^{-1} while the structurally characterized Fe(η^2-C(O)CH$_2$CMe$_3$)Br(CO)dippe has analogous bands at 1908 and 1591 cm^{-1}. The qualitative pattern of the shift in the terminal ν_{CO} frequencies and the 43 cm^{-1} difference in acyl ν_{CO} frequencies between η^1- and η^2-acyl complexes are comparable to those observed for $\mathbf{A_{Co}}$ and $\mathbf{I_{Co}}$. Such spectral observations are consistent with, but do not prove, the assignment of $\mathbf{I_{Co}}$ (and $\mathbf{I'_{Co}}$) as having the **C** conformation.

Notably, the terminal ν_{CO} shifts between the IR spectrum of $\mathbf{A_F}$ and the TRIR spectrum of $\mathbf{I_F}$ in DCE are similar, but the shift in the acyl ν_{CO} in that case (16 ± 3 cm^{-1}) is much smaller. This may imply that the electron-withdrawing nature of the CF$_3$ decreases the basicity of the acyl carbonyl so that η^2-coordina-

(46) Kelly, J. M.; Long, C.; Bonneau, R. *J. Phys. Chem.* **1983**, *87*, 3344−3349.

(47) Owing to the limitations of the TRIR apparatus, the upper limit for k_{CO} in THF was determined to be <5 × 10^2 M^{-1} s^{-1}, which is an order of magnitude slower than the k_{CO} values measured in CH$_2$Cl$_2$ or cyclohexane. However, for the faster reaction with P(OMe)$_3$ ($\mathbf{I_{Mn}}$ + L → Mn(CO)$_3$L(C(O)CH$_3$)) the k_L value in THF (1.7 × 10^3 M^{-1} s^{-1}) was 3 orders of magnitude slower than that in cyclohexane (1.4 × 10^6 M^{-1} s^{-1}).[23]

(48) Sweany, R. L.; Russell, F. N. *Organometallics* **1988**, *7*, 719−727.

(49) Versluis, L.; Ziegler, T.; Baerends, E. J.; Ravenek, W. *J. Am. Chem. Soc.* **1989**, *111*, 2018−2025.

(50) Versluis, L.; Ziegler, T. *Organometallics* **1990**, *9*, 2985−2992.

(51) Sola, M.; Zeigler, T. *Organometallics* **1996**, *15*, 2611−2618.

(52) Hermes, A. R.; Girolami, G. S. *Organometallics* **1987**, *7*, 394−401.

(53) Durfee, L. D.; Rothwell, I. P. *Chem. Rev.* **1988**, *88*, 1059−1079.

tion is no longer found. Since it is unlikely that the CF_3 group of I_F participates in agostic bonding as in **B**, this leaves **S** as the remaining option. The 15-fold greater reactivity of I_F with CO would be consistent with this intermediate being less stabilized than I_{Co}.

Dynamics of Methyl Migration and CO Trapping Reactions of I_{Co}. The kinetics data described above clearly emphasize a major difference between I_{Co} and the manganese analogue I_{Mn}. The reactivity of the former both toward CH_3 migration and toward trapping by CO is much higher, which may be one reason the cobalt carbonyls are an effective industrial carbonylation catalyst. For example, the k_M for I_{Co} in 25 °C benzene is 6.2×10^4 s^{-1} and that for k_{CO} is 1.1×10^7 M^{-1} s^{-1} while the respective values for I_{Mn} are 6.7 s^{-1} and 3.3×10^3 M^{-1} s^{-1}.

Although the absolute reactivities of the two intermediates are considerably different, the patterns show some important analogies. For most of the solvents the k_{CO} values for I_{Co} and I_{Mn} do not vary significantly with the donor nature of the solvent (the exception being THF with the latter). It is this observation that was viewed above as indicating an internally stabilized structure for I_{Co} (**B** or **C**). However, for both I_{Co} and I_{Mn}, the solvent appears to play a role in the methyl migration pathway. For example, with I_{Mn}, k_M is 50-fold higher in DCE than in perfluoromethylcyclohexane (PFMC) and this could be interpreted either in terms of the transition state being more polar than I_{Mn} (thus, the rate is accelerated by the more polar medium) or in terms of a more specific solvent metal interaction. The latter argument, but not the former, is consistent with the k_M being at least 10-fold larger in cyclohexane than in PFMC for I_{Mn}. The pattern for I_{Co} is similar; k_M follows an order (THF > DCE > CH_2Cl_2 > benzene) more or less consistent with the polarity and/or donor ability of the solvent. If both I_{Mn} or I_{Co} are primarily present as η^2-acyl complexes, the solvent effects on k_M may reflect the need for the acetyl group to rearrange to a transition-state configuration for acyl-to-methyl migration that is likely to resemble **B**. This might be assisted by direct interaction of the solvent with the metal center (the interpretation we have favored)[22] or by stabilization owing to changes in molecular polarity during this rearrangement.

The activation parameters reported here for CO trapping of I_{Co} in benzene indicate a very small activation enthapy (+6 kJ mol^{-1}) but a substantially negative activation entropy (−91 J mol^{-1} K^{-1}) for k_{CO}. This suggests that addition of CO to this intermediate has considerable associative character, perhaps a concerted displacement of the acyl oxygen with formation of the Co−CO bond. The "unimolecular" k_M pathway displays a higher $\Delta H^{\ddagger}_M$ (+40 kJ mol^{-1}) but a less negative $\Delta S^{\ddagger}_M$ (−19 J mol^{-1} K^{-1}). The negative $\Delta S^{\ddagger}$ may reflect the more organized nature of the solvation required to effect rearrangement of **C** to an acyl configuration more compatible with CH_3 migration to the metal.

Another model for migratory insertion that we and others have studied in some detail is concerned with the mechanism of CpFe(CO)(L)(C(O)CH$_3$) formation (L = CO or PR$_3$) from the methyl analogue CpFe(CO)$_2$CH$_3$ (M_{Fe}). The response of the ν_{CO} values and of k_L and k_{CO} to solvent donor properties first led to the conclusion the I_{Fe} has the solvento structure **S** for the donor solvents THF and acetonitrile and possibly in the chloroalkane and alkane solutions.[26] Methyl migration is also suppressed in THF and CH_3CN, unlike the patterns for I_{Mn} and I_{Co} where more polar solvents tend to increase k_M. The situation in alkane solutions is more ambiguous. The shift in the acyl ν_{CO} from A_{Fe} to I_{Fe} is the same (−70 cm^{-1}) for cyclohexane

Scheme 4

and for PFMC, and k_M values (25 °C) in these solvents are nearly identical, although the latter solvent is unlikely to form a stable metal−solvent complex. Temperature-effect studies in cyclohexane show $\Delta H^{\ddagger}$ and $\Delta S^{\ddagger}$ values of 44 kJ mol^{-1} and −5 J K^{-1} mol^{-1} and 34 kJ mol^{-1} and −28 J K^{-1} mol^{-1} for k_M and k_{CO}, respectively. The near-zero $\Delta S^{\ddagger}_M$ value for I_{Fe} is suggestive of a concerted CH_3 migration pathway perhaps from an agostic intermediate. Thus, an η^2-acyl-stabilized species analogous to **C** does not appear to play a role in this case.

When one considers the systems that have been subjected to time-resolved spectroscopic techniques to probe the reactive unsaturated intermediates in migratory insertion, the absence of a single dominant pattern is frustrating. With regard to structures, it appears that the model I_{Mn} and I_{Fe} complexes form the solvento species in stronger donors such as THF but are stabilized by the acetyl group in weakly donating solvents such as alkanes. For I_{Mn} such stabilization appears to take the form of η^2-coordination of the acyl carbonyl and this pattern appears to be paralleled by the catalytically important I'_{Co} and I_{Co}. Acyl stabilization of I_{Fe} under such conditions may be different, namely, agostic coordination of the CH_3. The data are not unambiguous regarding the relative energies of these acyl-stabilized intermediates. Perhaps this should not be surprising given the NMR studies by Carmona et al., which showed the acyl complexes Mo(C(O)CH$_3$)(S$_2$CX)(CO)(PMe$_3$)$_2$ to be present in a labile equilibrium between several such forms.[54] Thus, one is drawn to conclude that under certain conditions there may be a fine balance among the **C**, **S**, and **B** type configurations of these unsaturated intermediates and that the specific energetics favoring one or another may reflect subtle shifts in experimental conditions (Scheme 4).

Thermal kinetics studies of RC(O)Co(CO)$_3$L (R = alkyl) using in situ IR[10,12] and NMR[6,11] techniques have reported an inverse dependence on [CO] for the rates of CO exchange, reaction with H$_2$, and isomerization of R. The unsaturated intermediate RC(O)Co(CO)$_2$L has been invoked in mechanism discussions (e.g., eqs 3 and 4), but these techniques could not

$$CH_3C(O)Co(CO)_4 \underset{k'_{-CO}[CO]}{\overset{k'_{-CO}}{\rightleftarrows}} CH_3C(O)Co(CO)_3 + CO \quad (3)$$

$$CH_3C(O)Co(CO)_3 \underset{k'_{-M}[CO]}{\overset{k'_M}{\rightleftarrows}} CH_3Co(CO)_4 \quad (4)$$

probe the spectra or dynamics of this species directly. For example, Roe used high-pressure NMR magnetization exchange experiments[11] to determine activation parameters for CO loss from A'_{Co} in methylcyclohexane-d_{14} as $\Delta H^{\ddagger} = 92$ kJ mol^{-1}, $\Delta S^{\ddagger} = 33$ J mol^{-1} K^{-1} and suggested that the transition state for CO dissociation involved concerted coordination of the acyl

(54) Carmona, E.; Contreras, L.; Poveda, M. L.; Sanchez, L. J. *J. Am. Chem. Soc.* **1991**, *113*, 4322−4324.

oxygen. Although $\mathbf{I'_{Co}}$ was not detected in these experiments, the data provide an estimate for the k'_{CO}/k'_M ratio of 21 for $\mathbf{I'_{Co}}$ at $T = 70$ °C. Extrapolation of the data from laser flash photolysis of $\mathbf{A_{Co}}$ in benzene to the same conditions predicts a similar branching k_{CO}/k_M ratio (31) for the PPh₃-modified reactive intermediate $\mathbf{I_{Co}}$. The similarity in these ratios of $\mathbf{I'_{Co}}$ and $\mathbf{I_{Co}}$ supports the interpretation that the flash photolysis of $\mathbf{A_{Co}}$ is accessing the same reactive intermediate as that generated thermally.

Summary

Scheme 4 outlines key aspects of the above discussion regarding the behavior of reactive intermediate(s) prepared by photodissociation of CO from $\mathbf{A_{Co}}$. This can also serve as a more generalized model for discussing the intermediates generated similarly from the iron and manganese complexes $\mathbf{A_{Fe}}$ and $\mathbf{A_{Mn}}$. Intermediate $\mathbf{I}$ (Scheme 2) can be considered to be an equilibrium ensemble of the three species $\mathbf{C}$, $\mathbf{S}$, and $\mathbf{B}$ from which methyl migration to form $\mathbf{M}$ or trapping with CO to form $\mathbf{A}$ occurs. For the solvents probed in the present system, the TRIR spectra are consistent with the conclusion that $\mathbf{C}$ is the most prevalent configuration of $\mathbf{I_{Co}}$. That $\mathbf{I_{Co}}$ is not predominantly $\mathbf{S}$ is substantiated by the insensitivity of k_{CO} to solvent donor properties. In contrast, it is clear that k_M is solvent-dependent in a manner that suggests a more intimate role of solvent in the methyl migration pathway, and this observation argues against $\mathbf{I_{Co}}$ being $\mathbf{B}$.

Thus, the formation of $\mathbf{A_{Co}}$ from $\mathbf{I_{Co}}$ appears to occur via the concerted displacement of the oxygen of the η^2-coordinated carbonyl via an associative reaction of CO with $\mathbf{C}$ (k^C_{CO}), and this view is substantiated by the large negative $\Delta S^‡$ of that step

in benzene solution. The solvent dependence of the k_M pathway may simply reflect the necessity of solvent association to facilitate the isomerization of $\mathbf{C}$ to $\mathbf{B}$. The former has the CH₃− in a stereochemical location unfavorable for migration, while the latter appears to be well on its way toward the formation of $\mathbf{M}$. Alternatively, $\mathbf{M}$ may be formed directly from $\mathbf{S}$ by a concerted step k^S_M. In these contexts, the behavior of $\mathbf{I_{Co}}$ parallels that of the manganese analogue $\mathbf{I_{Mn}}$.[23] However, the reaction rates of the former are orders of magnitude faster, consistent with the role of phosphine-modified cobalt carbonyls as carbonylation catalysts. Although in Scheme 4 arrows are drawn unidirectionally from $\mathbf{I}$ to $\mathbf{A}$ and from $\mathbf{I}$ to $\mathbf{M}$ to denote the decay of intermediates generated via a photoreaction, we believe it likely that the thermal alkyl carbonylation pathways relevant to the catalysis mechanisms are sampling analogous intermediates such that microscopic reversibility may be assumed.

Supporting Information Available: Figure S-1 showing step-scan FTIR spectra after flash photolysis of $\mathbf{A_{Co}}$ and Figure S-2 Eyring plots for k_M and k_{CO} pathways. This material is available free of charge via the Internet at http://pubs.acs.org.

IC000378Y